Zwitterionic Ligand Capping for High Performance and Stable Perovskite Quantum Cutters

Yao Jing[1,2,3], Andre K. Y. Low[1,4], Yun Liu[5], Minjun Feng[6], Jia Wei Melvin Lim[6], Siow Mean Loh[7], Quadeer Rehman[1], Steven A. Blundel[7], Nripan Mathews[1,3], Kedar Hippalgaonkar[1,4], Tze Chien Sum[6*], Annalisa Bruno[1,3,6,*] and Subodh G. Mhaisalkar[1,3,8*]

[1]*School of Materials Science and Engineering, Nanyang Technological University, 50 Nanyang Avenue, Singapore 639798*

[2]*Collaborative Initiative, Interdisciplinary Graduate Programme, Nanyang Technological University, Singapore 637335*

[3] *Energy Research Institute @Nanyang Technological University (ERI@N), Research Techno Plaza, 50 Nanyang Drive, Singapore 637553*

[4]*Institute of Materials Research and Engineering (IMRE), Agency for Science, Technology and Research (A*STAR), 2 Fusionopolis Way, Innovis #08-03, Singapore 138634,*

[5]*Institute of High Performance Computing (IHPC), Agency for Science, Technology and Research (A*STAR), 1 Fusionopolis Way, #16-16 Connexis, Singapore 138632*

[6] *School of Physical and Mathematical Sciences, Nanyang Technological University, 21 Nanyang Link, Singapore 637371*

[7]*Université Grenoble Alpes, CEA, CNRS, IRIG, SyMMES, F-38000 Grenoble, France*

[8]*SKKU Institute of Energy Science and Technology (SIEST), Sungkyunkwan University, 2066, Seobu-ro, Jangan-gu, Suwon-si, Gyeonggi-do, Korea*

* subodh@ntu.edu.sg (S.M.), annalisa@ntu.edu.sg (A.B.), tzechien@ntu.edu.sg (T.C.S.)

Abstract

Quantum cutting (QC) shows significant potential in light-harvesting applications in view of its excellent downconversion ability that allows the conversion of high-energy photons into lower-energy photons, which may be more amenable to infrared communications. Yb-doped perovskite nanocrystals are reported to achieve efficient QC process with extremely high photoluminescence quantum yield (PLQY) thanks to the favorable Yb^{3+} incorporation in perovskite structure. However, conventionally used oleic acid–oleylamine based ligand pairs are known to cause instability issues due to highly dynamic binding to surface states that have curbed their potential applications. Herein, long-chain zwitterionic type C3-sulfobetaine 3-(N,N-Dimethylpalmitylammonio)propanesulfonate molecule is utilized to build a strong binding state on the nanocrystals' surface through a new phosphine oxide synthesis

route. Leveraging machine learning and Bayesian Optimization workflow to rapidly discover optimal synthesis conditions instead of time- and labor-intensive experimentation, ultrahigh near-infrared photoluminescence quantum yield (PLQY> 190%) is rapidly achieved. The high PLQY is well maintained after more than three months of storage, high-flux continuous UV irradiation and long-time continuous annealing. This is the first report of highly efficient and stable perovskite quantum cutters, which should eventually support the exploration of fundamental physics behind QC and near-infrared quantum communications.

Introduction

Quantum cutting (QC) is an appealing energy conversion process wherein a single high-energy photon is transformed into two lower-energy photons. This process holds great promise in enabling applications in low-energy illumination and quantum communications as well as improving the power conversion efficiency of photovoltaic (PV) devices.[1-4] Recently, Yb-doped $CsPb(Cl_xBr_{1-x})_3$ perovskite nanocrystals (NCs) were reported to realize an effective QC process.[5-9] As compared to the other host materials (colloidal $NaYF_4$, LaF_3, and related insulator NCs), the perovskite structure has a higher affinity for Yb^{3+} due to the favored Yb^{3+} incorporation and the soft nature of perovskites.[10-12] The sensitized Yb emission has demonstrated a high photoluminescence quantum yield (PLQY) of over 190% due to the efficient exciton-to-dopant energy transfer.[6-7] The sensitized f-f transition of Yb^{3+} in perovskite host located at near-infrared (NIR) region (~980nm) aligns well with the bandgap of silicon (~1.1ev), which has shown great potential in solar spectral shift applications.[13-14] In addition, NIR light-emitting diodes with emission wavelength over 800nm were also achieved through Yb-doped perovskite NCs, extending the application of perovskite NCs to optical communication, night-vision devices, and biomedical imaging.[15-16]

Although extremely high quantum yield (>100%) has been realized in Yb doped perovskite NCs through the QC process, these doped perovskite NCs with widely-used ligands pair of oleylamine (OAm) and oleic acid (OA) still suffer from severe stability problems.[17] The proton exchange process between OA and OAm molecules and thus the formation of neutral complex ($OAmH^+ + OA^- \rightleftharpoons -COOH_3NCH_2-$) leads to the rapid detachment of ligands from the nanocrystal's surface during purification and storage, resulting in poorer stability and deteriorated emission performance.[18-24] Besides, this highly dynamic ligands binding of OA and OAm pairs also brings about the loss of structural integrity, such as the sintering between perovskite NCs, creating more trap states and hindering its further applications.[25]

Therefore, employing a single ligand which possesses stronger binding with NCs' surface and doesn't generate neutral complexes could overcome the stability issues. Recently, zwitterionic molecules, that carry both cation and anion functional groups, have shown great potential in preserving structural integrity as well as excellent quantum efficiency of perovskite NCs.[25-28] Cohen et al. employed zwitterionic functionalized polymers to encapsulate the Yb doped $CsPbCl_3$ NCs through ligand

exchange method.[29] The NC/polymer composites still retained nearly the same PLQY for over 1.8 years of dark storage. However, the ligands-exchange procedure is complicated that required polymer synthesis and suitable solvent selection. More importantly, the surface states may be altered during the ligands-exchange process, causing more trap states and thus degrading the performance. Consequently, developing an in-situ synthesis method with stronger binding ligands is pressing for perovskite quantum cutters.

In this work, we demonstrate an in-situ phosphine oxide synthesis route to prepare robust and highly efficient Yb doped perovskite $CsPbCl_3$ NCs through zwitterionic type 3-(N,N-Dimethylpalmitylammonio)propanesulfonate (ASC-16) ligands. Tri-n-octylphosphine oxide (TOPO) was employed to assist the dissolution of $YbCl_3 \cdot 6H_2O$ precursor, which plays a critical role for effective Yb doping. Moreover, we replaced the traditional trial-and-error approach involving time- and labor-intensive experimentation using Bayesian Optimization (BO) to optimize for NIR photoluminescence quantum yield (PLQY) through QC process. Across only 2 iterations of the active learning process, we were able to rapidly discover NCs with ultrahigh NIR PLQY close to QC limit (~192±5%), which is one of the highest for Yb doped perovskite NCs ever reported. Due to the strong coordination between zwitterionic ligands and NCs' surface revealed by density functional theory (DFT) calculations, the prepared Yb doped $CsPbCl_3$ perovskite NCs exhibits greatly improved stability under high UV laser flux, continuous annealing, and also long-term colloidal storage stability even at Singapore's humid environment (at least three months). To the best of our knowledge, our work represents the first demonstration of achieving a high NIR PLQY close to the QC limit alongside exceptional stability in Yb-doped perovskite nanocrystals.

Results and Discussion

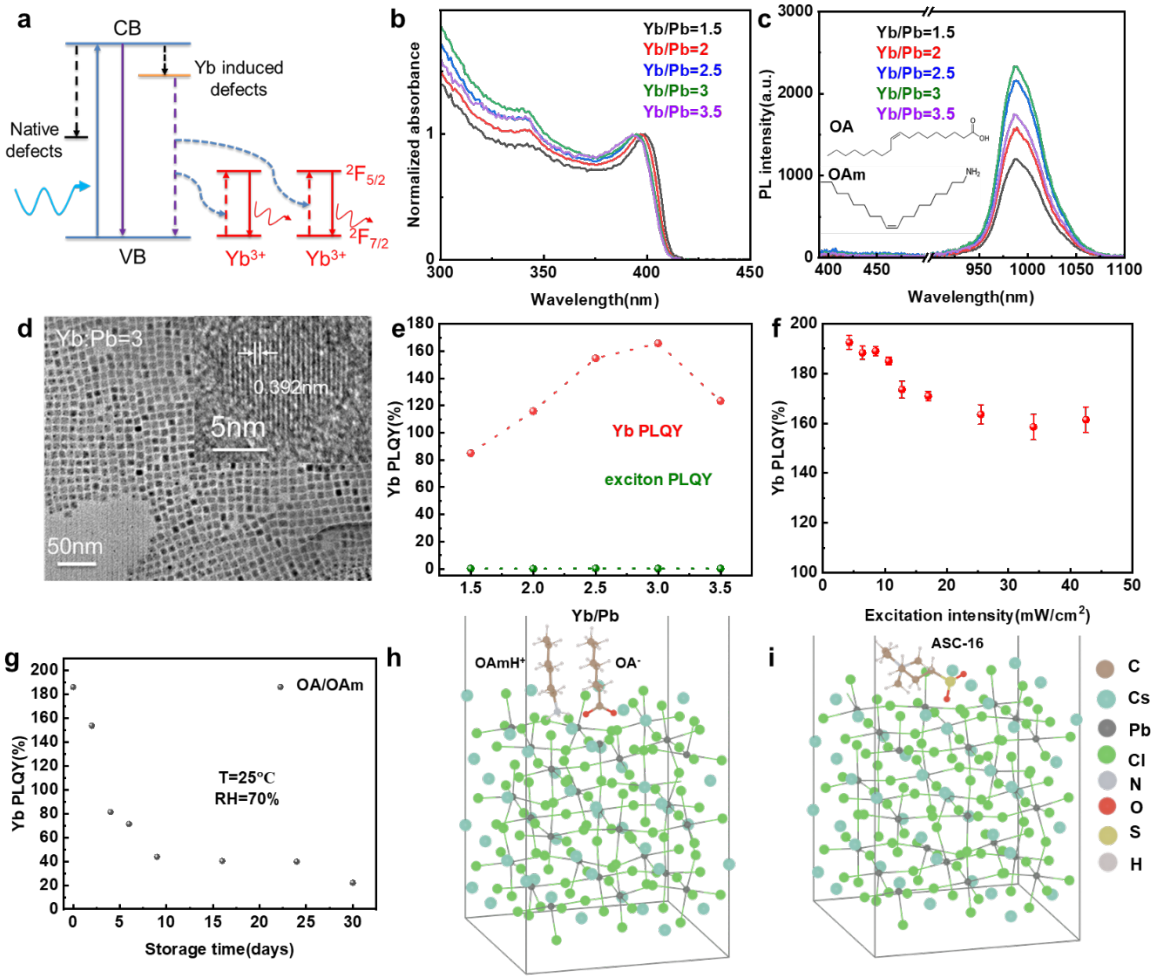

Figure 1. (a) Schematic of the quantum cutting process in Yb doped perovskite NCs. (b) Absorption (c) PL spectra of Yb doped $CsPbCl_3$ perovskite nanocrystals synthesized with different $YbCl_3{\cdot}6H_2O$ precursor amount. (d)TEM and HR-TEM image of Yb doped $CsPbCl_3$ NCs. (e) PLQY value of Yb doped $CsPbCl_3$ perovskite nanocrystals synthesized with different $YbCl_3{\cdot}6H_2O$ precursor amount. (f) Yb PLQY of optimal Yb doped NCs as the function of different excitation fluence. (g) Stability of Yb doped $CsPbCl_3$ NCs at ambient conditions. Calculated adsorption structures of (h) OA^-OAmH^+ (binding affinity: 2.57 eV) and (i) ASC-16(binding affinity: 2.92 eV) on a Cs-Cl terminal surface with a CsCl Schottky defect pair.

The schematic of QC process in Yb doped perovskite nanocrystals (NCs) is presented in Figure 1a. After photon excitation, the excited electrons in the conduction band would be trapped in the deep trap states caused by the Yb induced defects in the perovskite host.[30] Subsequently, the trapped electrons in the defect states would recombine with holes in the valence band, and the released energy would be transferred to two neighboring Yb ion simultaneously and populate the $^2F_{5/2}$ state. These two excited Yb ions would emit two NIR photons, completing the QC process. To achieve an efficient QC process, the host material bandgap must exceed twice the PL energy of Yb. Therefore, for lead halide perovskite, $CsPbCl_3$ and $CsPb(Cl_{1-x}Br_x)_3$ are usually utilized as the host materials to achieve the QC process. Herein, we used

$CsPbCl_3$ NCs as the host materials to investigate the energy transfer mechanism for QC as well as the stability issues.

Firstly, we tried to realize the QC phenomenon in Yb doped $CsPbCl_3$ perovskite NCs using oleic acid (OA) and oleylamine (OAm) capping ligands pair. To explore the synthetic conditions for Yb doped $CsPbCl_3$ NCs with the best performance, a series of comparison experiments were performed. We followed the optimization sequence shown in Figure S1. As demonstrated in Figure S2-S4, the reaction temperature and ligands amount play key roles in facilitating the incorporation of Yb^{3+} dopants into $CsPbCl_3$ perovskite host. It can be concluded that higher temperature promotes Yb incorporation (above 260°C) and OA/OAm ligands can passivate the defects and facilitate the Yb doping (Figure S2). The ratio of OA/OAm amount should be kept at 1 and excess OAm amount might lead to the generation of low dimensional products (nanoplatelets,etc.) due to the competition between Cs^+ and NH_3^+, which degraded the Yb emission performance (Figure S3).[19] Interestingly, Cs/Pb feeding ratio has no remarkable influence on Yb^{3+} doping (Figure S4).

After determination of the optimized synthesis conditions in terms of the ligands proportion, reaction temperature, and Cs/Pb ratio, the overall synthesis procedure was optimized with different Yb precursor amount to achieve the highest Yb emission efficiency. Figure 1b shows the absorption spectra of Yb-doped samples with different ytterbium precursors. The absorption curves exhibit a slightly blue shift when increasing the amount of Yb precursor, which can be attributed to the reduced lattice parameters as the radius of Yb is smaller than Pb. The narrower lattice can increase the band gap, which leads to this slightly blue shift.[31] In PL spectra, all Yb-doped samples show very weak exciton emission from the perovskite host, indicating a new energy relaxation channel after Yb doping (Figure 1c). The Yb emission peak around 980 nm becomes stronger increasing the amount of Yb precursor during the synthesis, which is caused by increased Yb doping amount in the lattice. All samples show uniform cubic shapes around 9 nm. From the size distribution graph, it can be observed that the average size nearly remains constant when increasing the Yb precursor amount during synthesis (Figure 1d and S5). The highest PLQY is achieved at the nominal ratio of Yb to Pb of 3 during synthesis and the PLQY is close to 170% (Figure 1e). The real Yb doping concentration is around 3.1% determined from the Inductively Coupled Plasma Optical Emission Spectroscopy (ICP-OES) (Table S1). Such high PLQY exceeds 100% suggesting that quantum-cutting is taking place in the Yb emission process. The PLQY was also measured with reduced excitation powers to metigate the Auger effect during the quantum-cutting process.[32] As shown in Figure 1f, the Yb PLQY value can reach ~190% at the lowest excitation rate, close to the quantum cutting limit (200%). This pretty high PLQY also indicates the high quality of the synthesized Yb-doped $CsPbCl_3$ nanocrystals sample in this study. When the amount of Yb increases, X-ray diffraction (XRD) peaks show a slight shift to higher degrees, and the width of the peak becomes broader, suggesting the replacement of Pb with Yb and reduced crystallinity after Yb doping (Figure S6).[31]

Although excellent quantum efficiency has been achieved with conventional OA/OAm ligands pair, the highly dynamic ligands binding makes these NCs unstable. The bounded ligands are easy to desorb from the NCs' surface, creating trap states and

degraded performance. The moisture environment accelerates this degradation, as shown in Figure 1g. During storage in ambient conditions, the PLQY of Yb doped $CsPbCl_3$ NCs decreased greatly, to ~40% only after 7 days, suggesting the decomposition of perovskite structure caused by ligands detachment since no absorption peak was observed (Figure S7). Consequently, selecting new generation ligands is urgent for perovskite quantum cutters to enable high efficiency as well as structural integrity.

With the aim of stronger binding and avoiding the generation of neutral complex, a zwitterionic C3-sulfobetaine molecule (3-(N,N-Dimethylpalmitylammonio)propanesulfonate, ASC-16) was selected to act as capping ligands for $CsPbCl_3$ perovskite host. To better understand the interaction between traditional $OAmH^+OA^-$, ASC-16 ligands and NCs' surface, DFT calculations were performed based on a CsCl-rich (100) surface of $CsPbCl_3$ with either $OAmH^+OA^-$ or ASC-16 passivation (Figure 1h,i). Due to the large computational cost of the long carbon chain of the ligands, we created representative shorter chain counterpart with the same functional group as the ASC-16, OA and OAm ligands. Meanwhile, Yb ions were not included in the perovskite due to the low Yb doping concentration. The most stable CsCl Schottky defect pair configuration was used to represent the surface defects in perovskite NCs and served as the starting structure for ligands passivation (Figure S8). For zwitterionic ASC-16 ligands, the cation group occupied Cs^+ vacancy and bound with Cl ions through hydrogen bond while the anion group occupied Cl vacancy and interacted with Pb atoms. This chelating effect results in a larger binding affinity (2.92 eV) of ASC-16 compared to that of the $OAmH^+OA^-$ ligands pair (2.58 eV). The stronger binding affinity indicates that ASC-16 can act as an efficient chelating ligand to stabilize $CsPbCl_3$ perovskite NCs.

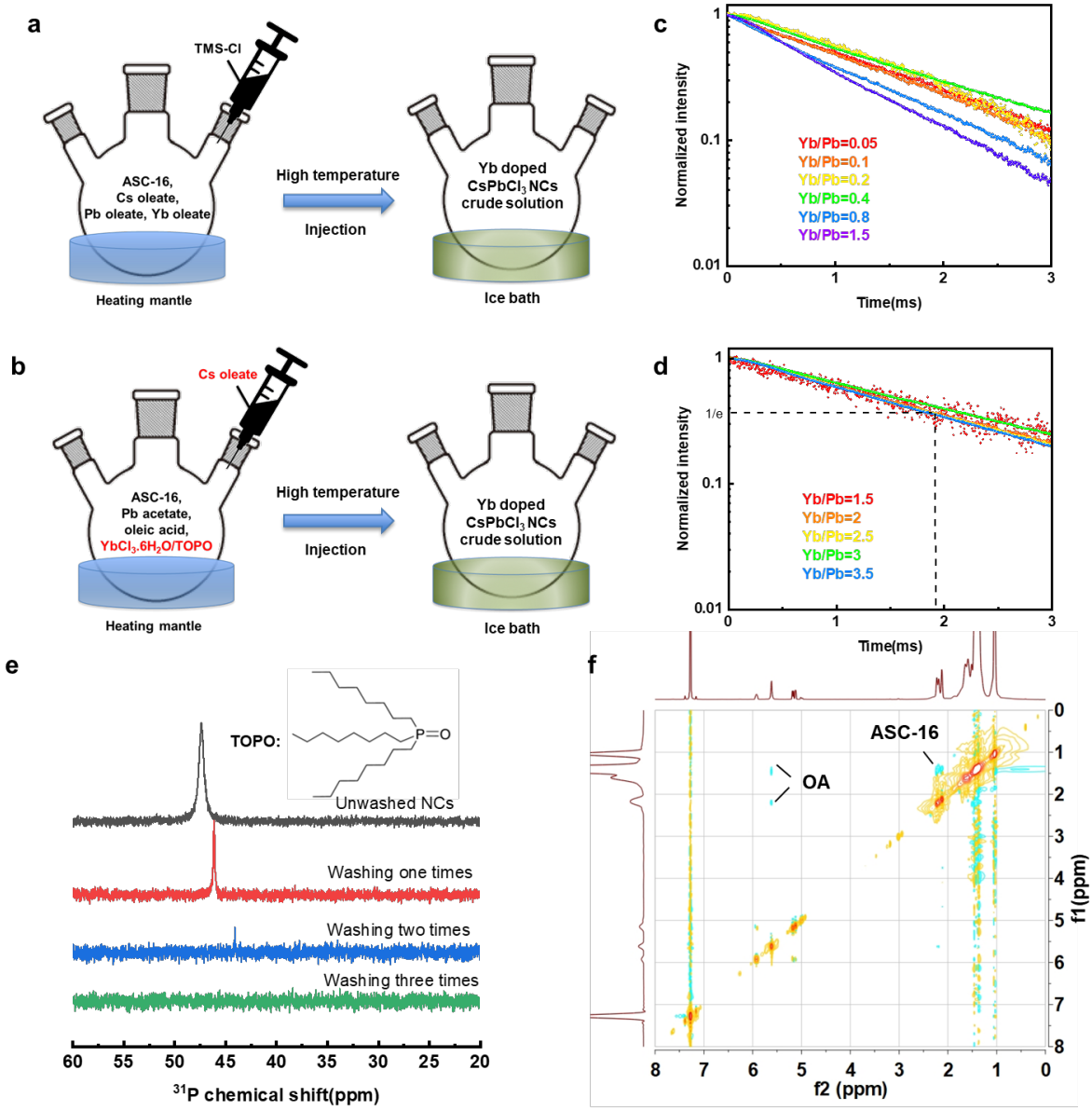

Figure 2. Synthesis procedures of Yb doped $CsPbCl_3$ nanocrystals with ASC-16 ligands (a) oleate precursor route; (b)$YbCl_3{\cdot}6H_2O$/TOPO route. (c,d) Yb emission lifetime as the function of Yb precursor amount during synthesis. (e) Solution ^{31}P NMR spectra for Yb doped $CsPbCl_3$ NCs with different washing times. (f)1H NOESY NMR spectrum of purified Yb doped $CsPbCl_3$ nanocrystals using $YbCl_3{\cdot}6H_2O$/TOPO synthesis route.

Selecting suitable precursors is crucial to realize effective Yb incorporation into lattice and obtain high quantum efficiency. The currently reported works all adopted oleate salt synthesis route when employing zwitterionic ligands. We also tried to do Yb doping through Yb oleate precursor (Figure 2a). However, the Yb PLQY did not exhibit continuous increasement when increasing the Yb oleate amount, indicating an insufficient Yb doping (Figure S9). To achieve effective Yb incorporation, we developed a new phosphine oxide synthesis route where $YbCl_3{\cdot}6H_2O$ was employed as Yb precursor instead of Yb oleate (Figure 2b). Meanwhile, TOPO was added to assist the dissolution of $YbCl_3{\cdot}6H_2O$ due to the combination of oxygen and ytterbium

atoms (Figure S10). OA was added to regulate the growth of NCs as well as adjust the solubility of Pb acetate and ytterbium chloride.[33]

To confirm whether Yb incorporated into the crystal, time-resolved photoluminescence lifetime (TRPL) measurements of Yb emission were conducted. For the Yb oleate precursor synthesis route, the Yb PL decay evolved from single exponential to biexponential as increasing the Yb oleate amount during the synthesis (Figure 2c, Table S2). The reduced emission lifetime was caused by the multiphonon relaxation involving C−H (~3000 cm^{-1}) or O−H (~3300 cm^{-1}) bonds vibrations as Yb emission energy (~10 000 cm^{-1}) takes only 3 or 4 vibrational quanta of these chemical bond to bridge the energy gap of 4f-4f transition, suggesting some Yb^{3+} ions just replaced some surface ions and coordinated with organic ligands rather than incorporated into the crystal. [10-11, 34] In contrast, the samples with different Yb concentration based on our new synthesis route all exhibit ~2ms single exponential decay from Yb^{3+} ion $^2F_{5/2} \rightarrow {}^2F_{7/2}$ transition, confirming more effective Yb doping into crystal (Figure 2d). This effective doping was also confirmed by ICP-OES tests as higher Yb doping concentration (~6.19%) was achieved compared with routine oleate precursor synthetic route (Table S3 and S4).

Solution Nuclear Magnetic Resonance (NMR) spectroscopy was carried out to study the interaction between ligands and NCs' surface. Figure 2e shows the ^{31}P NMR spectra of Yb doped $CsPbCl_3$ NCs solution with different washing times. For the unwashed samples, there is a sharp peak between 45~50 ppm, attributable to TOPO molecule. Only after two antisolvent purification times, no ^{31}P signal was detectable, suggesting the weak binding states of TOPO molecule on the NCs' surface. However, after complete purification, boarded and shifted peaks belonging to ASC-16 molecule were still observed for colloidal NCs solution as compared to free ASC-16 molecule, confirming the strong binding between ASC-16 ligands and NCs' surface (Figure S11).[25] 2D Nuclear Overhauser effect NMR spectroscopy (NOESY) was also employed to confirm the binding ligands. As shown in Figure 2f, negative cross peaks from ASC-16 and OA were observed, indicating the binding state of ASC-16 ligand and also the presence of OA to passivate NCs' surface. The presence of OA ligands originates from the Cs oleate precursor during injection and the addition of OA to regulate the growth of NCs, which aligns well with previous research.[33, 35]

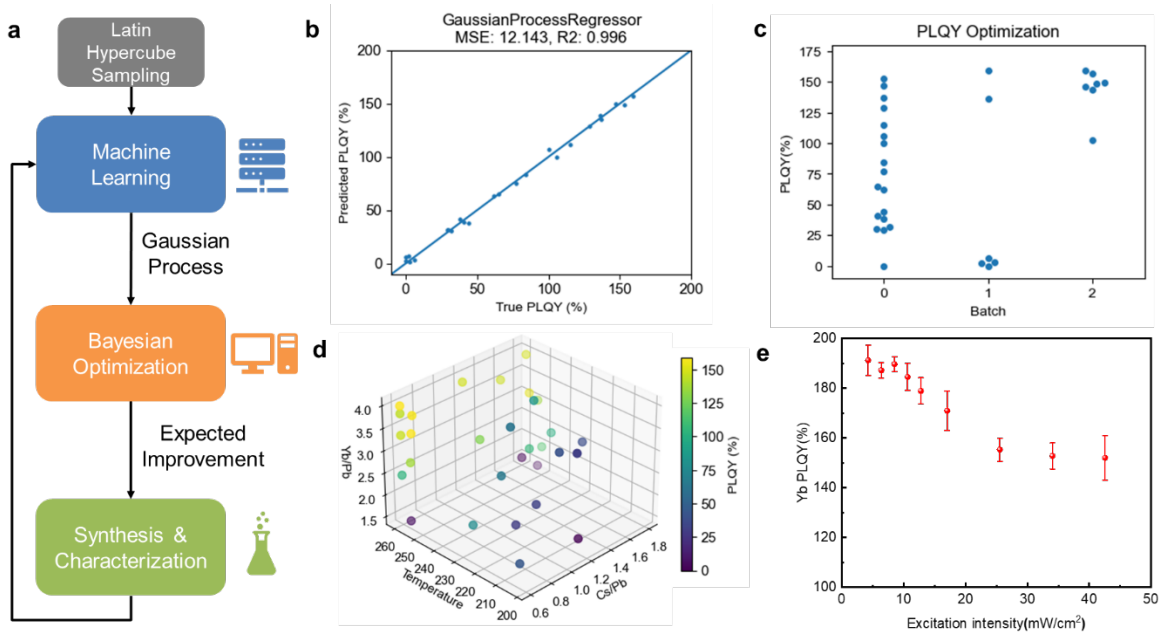

Figure 3. (a) ML and BO active learning workflow for optimizing PLQY of NCs, starting from initial sampling with LHS, followed by model training and implementing BO to propose samples. (b) Model accuracy for Gaussian Process Regressor after the 1st iteration, taking 24 data points, with MSE and R2 scores reported. (c) Evolution of PLQY across 2 iterations of BO as a swarm plot, with best value for each batch shown above. (d) 3D scatter plot for Yb/Pb, temperature and Cs/Pb variables, coloured by PLQY value. Highest PLQY values reported at top left corner corresponding to high Yb and high temperature. (e) Power-dependent PLQY measurements for the optimized sample by BO.

We then proceed to optimize for PLQY of Yb doped $CsPbCl_3$ NCs with this new synthesis route to attain robust quantum emitters. Here, we implemented Bayesian Optimization (BO), which relies on a predictive surrogate model paired with an acquisition function that determines which sample to evaluate next. BO lends itself as a suitable method for optimization in materials science where experiments are costly, owing to its sample efficient approach, with successful use cases across a variety of materials.[36-38] We initialized the optimization campaign using Latin Hypercube Sampling (LHS), implemented via scikit-optimize, providing 18 samples (parameters and measured PLQY are reported in Table S5). The constraints on parameters (ASC-16 amount, OA amount, Cs/Pb ratio, Yb/Pb ratio and reaction temperature) were defined empirically. Figure 3a reports the overall workflow of the optimization campaign. The initial dataset is used to train a Gaussian Process (GP) regressor, taking a Matern kernel.[39] The Expected Improvement (EI) acquisition function was chosen for selecting the next batch of candidates. The entire computational workflow is done in-the-loop using the gp_minimize function from the scikit-optimize library, taking default hyperparameters with no adjustments. We opted for gp_minimize which uses a GP surrogate model specifically, considering the cross-validated accuracy of different models (reported in Fig S12). The accuracy of the default GP model at the 1st iteration is also shown in Figure 3b.

In total, we performed 2 iterations of BO with 6 and 7 samples respectively to account for a reasonable turnaround time in synthesis and characterization of a batch samples. The results are reported in Figure 3c, where we were able to consistently attain samples with high PLQY (~160%) rapidly in only 2 iterations. We also furnish tables S6 and S7 in the supplementary to list out all the samples. Based on feature analysis (shown in Fig S13), we observed that temperature, Yb/Pb variables had the strongest correlation to PLQY and Cs/Pb ratio had no discernible impact on PLQY. Figure 3d shows a scatter plot of these variables with respect to PLQY, where the best samples occur in the region with high temperature, high Yb/Pb. We elucidate that this combination of parameters allows for overcoming the Yb doping energy barrier. Due to the large absorption cross section of $CsPbCl_3$ NCs, power-dependent PLQY measurements were carried out to minimize the nonradiative Auger loss following the active learning process. As shown in Figure 3e, highest NIR PLQY close to QC limit (~192±5%) was achieved at lowest excitation rates. This rapid exploration process for ultrahigh PLQY just after two iterations demonstrates the efficacy of BO for materials optimization.

Although the ASC-16 amount is weakly correlated with the emission efficiency of the doped NCs according to the feature analysis (Figure S13), the impact of ligands amount on the stability of the samples still needs to be explored. Consequently, the stability of Yb doped $CsPbCl_3$ NCs synthesized with different ASC-16 amount was investigated. As shown in Figure S14, under continuous UV laser irradiation, the photostability of samples improved gradually when increasing ASC-16 amount, indicating the protection of ligands shell. 25mg of ASC-16 ligand during synthesis is enough to prepare robust Yb doped NCs, which was employed for the following stability measurements.

The monodispersed Yb doped $CsPbCl_3$ NCs after BO optimization exhibit cubic shape and uniform size around 20 nm, as shown in Figure 4a. In-situ anion exchange was conducted to investigate the dependence of QC efficiency on the band gap of perovskite host. As increasing the adding amount of bromide precursor into pristine Yb doped $CsPbCl_3$ colloidal solution, we can observe an obvious band gap shift as the substitution of Cl with Br ions and the composition of perovskite host became $CsPb(Cl/Br)_3$ (Figure S15a). As the band gap decreases, the energy separation (Δ) between the CB minimum and trap state also decreases. This means that the electrons in the trap states can be reexcited to the CB minimum at room temperature, reducing the population of trap states and thus reducing the QC efficiency (Figure 4bii). Consequently, reduced Yb emission intensity can be monitored when increasing the Br concentration (Figure 4b, S15b). Smaller energy separation, weaker Yb emission. As the band gap of perovskite host decreases further below QC threshold ($2xE_{f\text{-}f}$), the Yb emission dropped significantly since the energy of excited electrons can only be transferred to one Yb ion rather than two Yb ions simultaneously, suggesting the termination of QC process (Figure 4biii). The dependence of Yb emission intensity on the band gap provides strong evidence that the NIR emission from our samples relies on the QC process.

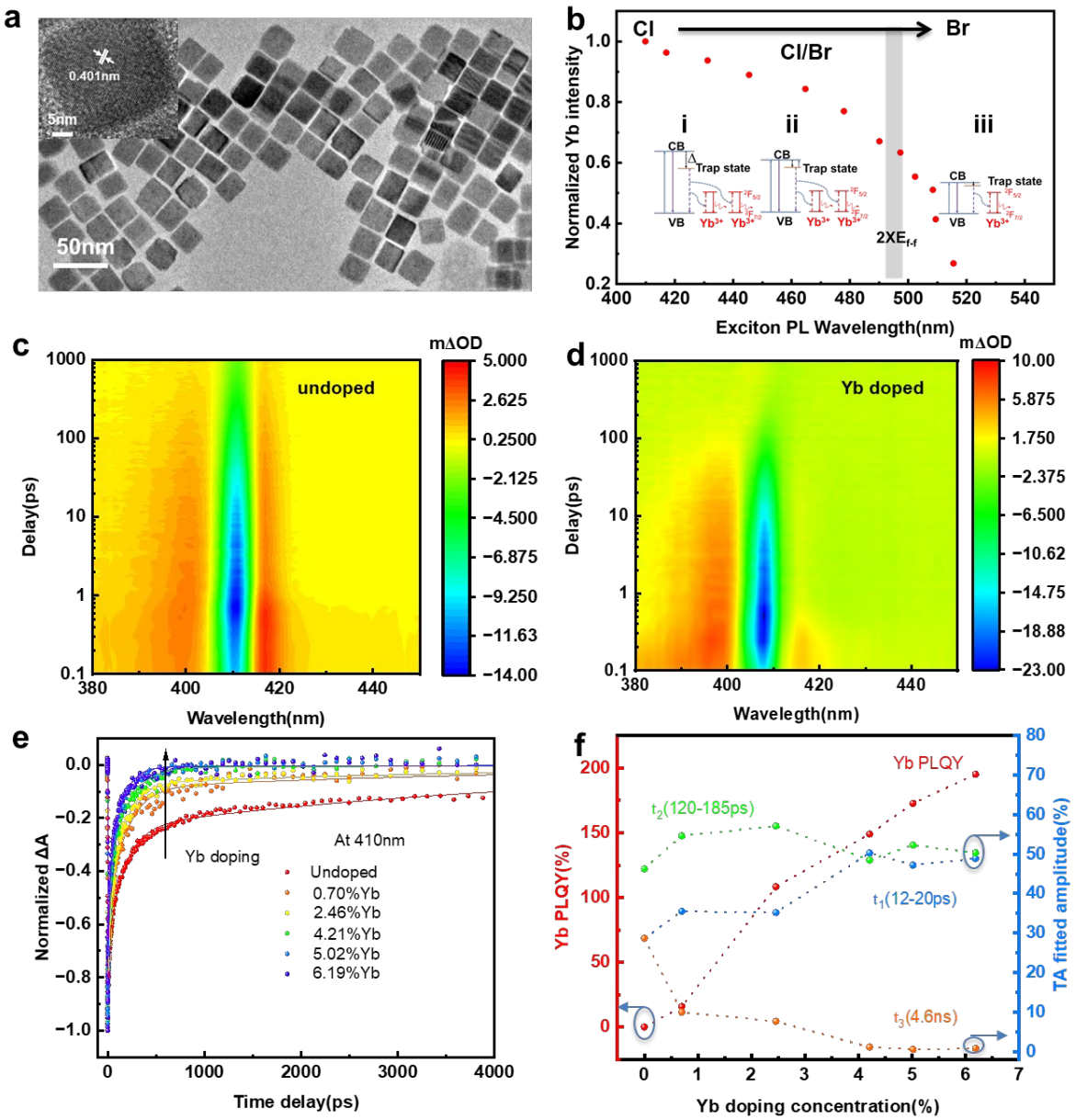

Figure 4. (a) TEM and HR-TEM image of optimized Yb doped $CsPbCl_3$ NCs with ASC-16 ligands. (b) Evolution of Yb emission intensity as function of exciton PL wavelength through in-situ anion exchange reaction. 2D contour plots of the TA spectra for (c) undoped and (d) Yb doped $CsPbCl_3$ NCs with ASC-16 ligands. (e) Normalized TA signal decay at 410 nm as a function of time for Yb-doped $CsPbCl_3$ nanocrystals with different real Yb doping concentrations. (f) Fitted TA amplitudes of different components plotted vs real Yb doping concentrations and Yb PLQY.

To investigate the dynamics of photoexcited carriers and energy transfer mechanisms for Yb emission, transient absorption (TA) spectroscopy was conducted for perovskite nanocrystals with different Yb doping concentrations. In Figure 4c, the TA spectra of undoped perovskite $CsPbCl_3$ nanocrystals exhibit an obvious bleaching signal at around 410 nm, which originates from the excitonic transition of the perovskite host. The decay of the absorption feature becomes faster with higher Yb concentration, indicating the introduction of a new relaxation channel upon Yb doped in the lattice

(Figure 4d,e, S16,S17). Moreover, these absorption decay can be fitted with three components (Table S8). The longest component (τ_1) at nanosecond timescale can be attributed to the radiative recombination of host materials, the amplitude of which becomes smaller as the increment of Yb doping amount, indicating the suppression of radiative recombination from perovskite host by Yb doping. On the other hand, the fastest one (τ_3) is more pronounced with higher Yb concentrations and higher Yb PLQY (Figure 4f), which can be assigned to the trapping process caused by Yb-induced defects. The formation of Yb-Pb vacancy-Yb structure may be responsible for this defect state.[30, 40] Therefore, the sensitized Yb emission stems from this ultrafast trapping process (~10 ps) and is then followed by the excitation of two neighboring Yb^{3+} ions simultaneously, completing the QC process. The similar energy transfer mechanism was also indicated by the faster TA decay for doped samples with OA/OAm ligands (Figure S18,S19). On top of this slow component (τ_1) and fast component (τ_3), the fitted TA decay dynamics also comprises another component (τ_2) with hundreds of picoseconds. To determine the origin of τ_2, power-dependent TA measurements were conducted for Yb-doped samples. It can be seen that the amplitude of τ_2 increases and the life becomes faster when increasing excitation power, indicating this component represents a typical Auger recombination process for the perovskite host (Figure S20, Table S9).[41]

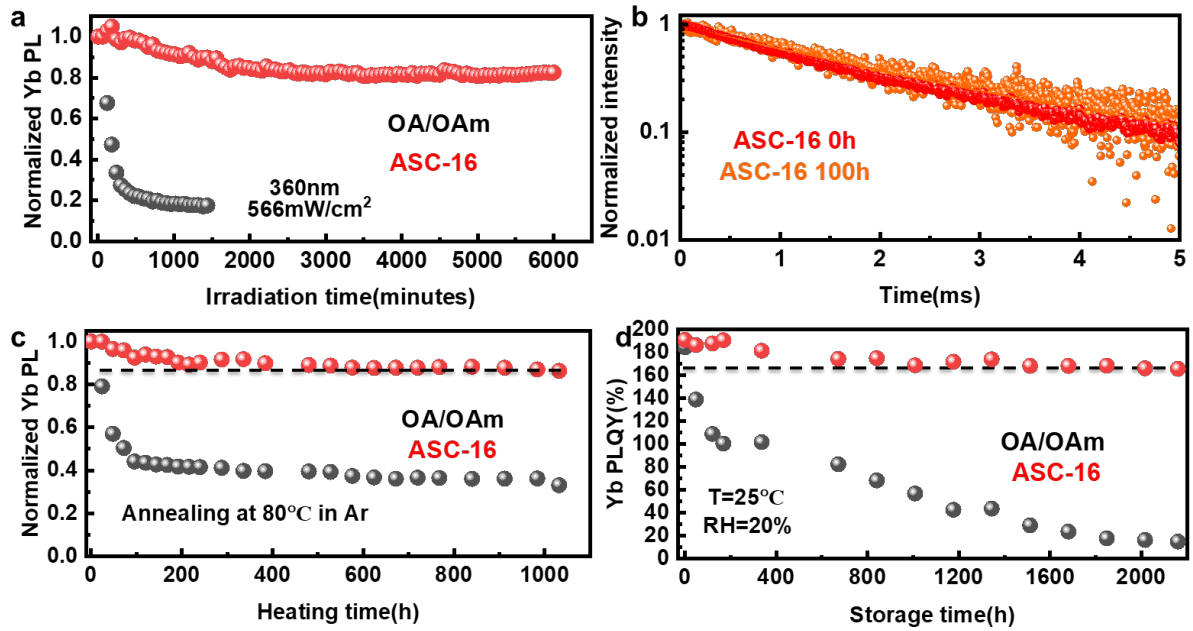

Figure 5. (a) Normalized Yb emission intensity as a function of irradiation time for Yb doped $CsPbCl_3$ NCs with traditional OA/OAm and ASC-16 ligands. (b)TRPL of Yb emission for Yb doped $CsPbCl_3$ NCs with ASC-16 ligands before and after exposed to UV irradiation. Relative PL intensity of Yb doped $CsPbCl_3$ NCs with different ligands (c) after annealing at 80°C in Ar atmosphere and (d) stored at controlled conditions (~25°C, ~20%RH).

Photostability is the key to its fundamental study as well as practical applications. Herein, the photostability measurement of Yb-doped perovskite $CsPbCl_3$ nanocrystals with zwitterionic ligands and traditional ligands was conducted to verify the stronger binding of ASC-16 ligands. Both samples were dispersed in toluene with the same

optical density (OD~0.3) and irradiated by 360 nm UV laser with the same power density (566 mW/cm^2). The Yb PL intensity as the function of irradiation time was recorded. As shown in Figure 5a and Figure S21a, for the sample with traditional OA/OAm ligands, the degradation occurs obviously as the PL intensity decreases greatly only after 10 h irradiation. The PL quenching can be explained by the photoinduced desorption of surface ligands, causing the aggregation between nanocrystals and more defect sites, which is confirmed by the red shift absorption peak and TEM measurements (Figure S22). The degradation of the perovskite host leads to more pronounced non-radiative recombination and thus suppresses the energy transfer process. However, the Yb-doped perovskite $CsPbCl_3$ nanocrystals with ASC-16 ligand exhibits robust properties against UV irradiation, which can still retain ~80% of its original PL intensity even after 100 h irradiation. We can still observe monodisperse NCs after long time irradiation rather than aggregation using traditional ligands pair (Figure S22). In contrast to the doped samples with traditional OA/OAm ligands, which exhibited a reduction in Yb emission lifetime after degradation (Figure S21b and Figure S23), indicating Yb ion migrates to the nanocrystals' surface due to crystal structure changes, the degraded Yb-doped $CsPbCl_3$ nanocrystals with ASC-16 ligands maintained a single exponential decay (Figure 5b). This suggests the preservation of structural integrity, highlighting the superiority of ASC-16 ligands in preventing adverse effects on the nanocrystal structure during degradation. Thermal stability was also evaluated to confirm the enhanced stability of ASC-16 capped NCs. As shown in Figure 5c and Figure S24, the ASC-16 capped Yb doped NCs still retained ~90% of its original PL intensity after 43 days continuous annealing. In contrast, the Yb emission intensity of OA/OAm capped NCs decreased by 63%. The absorption spectra of OA/OAm capped NCs also exhibits greater red shift than that for ASC-16 capped NCs (Figure S25), manifesting the strong binding effect of ASC-16 molecule on the NCs' surface.

In addition to the photostability and thermal stability problem, long-term storage stability is also an important issue that must be addressed for practical applications. On one hand, the highly dynamic ligand binding of OA/OAm ligands makes these NCs unstable. The decomposition occurs quickly and the humid environment usually aggravate this disadvantage, causing decreased energy transfer efficiency and quenched Yb emission. As shown in Figure S26, only after 4days, the PLQY of NCs capped with OA/OAm ligands dropped below 100% at ambient conditions (~70% RH, ~25 °C), indicating the absence of QC process due to the defects generation. After 30days, nearly no Yb emission was observed, suggesting the poor protection effect of highly dynamic binding ligands. In contrast to this disappointing performance, ASC-16 capped Yb doped NCs exhibited robust storage stability. Even under Singapore's humid environment, the colloidal solution still possesses high PLQY above 100% through QC process after 107 days storage. At controlled conditions (~25°C, ~20% RH, Figure 5d), ultrahigh PLQY was still obtained for the ASC-16 capped NCs even after 90 days while the OA/OAm capped Yb doped NCs still degraded quickly at reduced humidity environment.

Table 1. Best performance summary for Yb doped perovskite NCs.

Sample	Doping	Ligands	NIR PLQY	Stability	Reference
Yb:$CsPbCl_3$ NCs	Yb doping	OA, OAm	~ 190 %	/	[42]
Yb:$CsPbCl_3$ NCs	Yb doping	OA, OAm	167%	/	[31]
Yb:$CsPbCl_3$ NCs	Yb doping	OA, OAm	170%	/	[30]
Ce/Yb:$CsPbCl_{1.5}Br_{1.5}$ NCs	Ce/Yb Codoping	OA, OAm	115.5%	PL decreased less than 5% in the air for 700 h	[43]
Cr/Ce/Yb:$CsPbCl_3$ NCs	Cr/Ce/Yb tridoping	OA, OAm	175%	PL intensity decays 2% after 300 days	[44]
Yb:$CsPbCl_3$ NCs	Yb doping	OA, OAm	164%	/	[45]
Yb:$CsPbCl_3$ NCs	Yb doping	Poly(isopropyl methacrylate)	/	PL constant 1.8 years	[46]
Yb:$CsPbCl_3$ NCs	Yb doping	Zwitterionic type ASC-16	192±5%	PLQY >165% over 90days storage PL retains 80% after 6000mins continuous UV irradiation PL retains 86% after 1000h continuous annealing	This work

To date, many surface engineering methods have been proposed to improve the stability of perovskite NCs, including ligands engineering and surface coating. However, although ultra-high PLQY has been obtained for Yb doped perovskite quantum cutters, the widely used highly dynamic binding ligands still bring about instability issues. Despite polymer encapsulation has been employed to enhance the stability of perovskite quantum cutters, there are few reports of increased stability of Yb doped perovskite NCs with maintenance of high PLQY (Table 1). ASC-16 capped Yb doped perovskite $CsPbCl_3$ NCs not only possess high PLQY approaching QC limit, but also exhibit good resistance against humid environment, light irradiation and heat treatment, indicating their potential in fundamental study and practical applications.

Conclusion

In summary, we developed a ligands engineering method employing strong binding zwitterionic type C3-sulfobetaine (ASC-16) ligand through a new synthesis route, where TOPO was used to dissolve ytterbium halide precursor and thus enabling effective Yb doping. Bayesian Optimization was employed to discover the best conditions for Yb PLQY rapidly only after 2 iterations, which generated Yb doped NCs with ultrahigh NIR PLQY close to QC limit (~192±5%). Both the theoretical and experimental results confirmed the stronger binding strength between ASC-16 and NCs' surface due to the chelation effect. Yb doped $CsPbCl_3$ NCs capped by ASC-16 ligands show PLQY above 190%, excellent high-energy UV irradiation stability, good long-term storage stability, and robust thermal stability. Furthermore, it is possible to

extend our new synthesis route to achieve other exotic elements doping in perovskites. This work not only provides an in-depth understanding of the surface modification of doped NCs, but also facilitates efforts to study the fundamental physics behind QC and NIR quantum communications.

Experimental Section

Chemicals: Cesium carbonate (Cs_2CO_3, 99.999%), oleic acid (OA, 90%), oleylamine (OAm, 70%), methanol (99.8%, anhydrous), ethanol (99.9%, anhydrous), octadecene (ODE, 90%), ethyl acetate (99%, anhydrous), toluene (99.9%, anhydrous), Ytterbium(III) chloride hexahydrate ($YbCl_3.6H_2O$, 99.9%), ytterbium(III) nitrate pentahydrate ($Yb(NO_3)_3·5H_2O$, 99.9%), potassium oleate (KOA, 87%), 3-(N,N-Dimethylpalmitylammonio)propanesulfonate (ASC-16, 98%), chlorotrimethylsilane (TMS-Cl, 98%) were all purchased from Sigma-Aldrich. Lead acetate trihydrate ($Pb(OAc)_2·3H_2O$, 99.999%), Tri-n-octylphosphine Oxide (TOPO, >95.0%), cyclohexane (99%) and benzoyl bromide (>98.0%) were ordered from TCI, Japan. All chemicals were used directly without further purification.

Preparation of cesium oleate: 2.5 mmol Cs_2CO_3, 15 mL ODE and 1.25 mL OA were loaded into a 50 mL three-neck flask and then degassed at 120 °C until stopped bubbling. Subsequently, filled the flask with argon and heated it to 150 °C until all precursors dissolved completely and get a clear solution. This solution was pre-heated at 100 °C before use.

Preparation of lead oleate ($Pb(OA)_2$): 6mmol $Pb(OAc)_2·3H_2O$ (2.3033 g), 3.8 mL OA and 8.2 mL ODE were loaded in a 25 mL three-necks flask and then degassed at 120 °C until it stops bubbling. The precursor solution will become solid at room temperature and is needed to be preheated at 100 °C before use.

Preparation of ytterbium oleate ($Yb(OA)_3$): 4mmol $Yb(NO_3)_3·5H_2O$ (1.797 mg) was dissolved in 20 mL deionized water. 4 g KOA was dissolved in 20 mL deionized water and 25 mL ethanol mixture to get a clear solution. Then these two solutions were mixed and 50 mL cyclohexane was added to extract the $Yb(OA)_3$ by continuously stirring for 20 min. Subsequently, the upper cyclohexane layer containing $Yb(OA)_3$ were separated by a separatory funnel. 10 mL deionized water and 10 mL ethanol were added to wash it and also separated by a separatory funnel. This washing procedure was repeated by at least three times to remove the excess KOA. Finally, the cyclohexane in the upper organic layer was evaporated under vacuum at 80 °C and the $Yb(OA)_3$ was obtained.

Synthesis of Yb doped $CsPbCl_3$ perovskite nanocrystals with traditional OA/OAm ligands: 0.123 mmol $Pb(OAc)_2·3H_2O$, 10 mL ODE, 2 mL OA, 2 mL OAm and different amounts of $YbCl_3.6H_2O$ (Yb: Pb=1.5, 2, 2.5, 3, 3.5) in 1 mL methanol were loaded in a 25 mL quartz flask. This mixture was degassed at room temperature for 5 mins and then heated to 120 °C under vacuum for 1 h. Then, the flask was filled with argon and increased temperature to 260 °C quickly. 0.8 mL cesium oleate was injected swiftly and the flask was transferred to the ice bath to stop the reaction. After

the solution was cooled down to room temperature, the crude solution was centrifuged at 7500 rpm for 10 mins and collected the precipitate. The precipitate was dispersed in 3 mL toluene and centrifuged again at 10000 rpm for 8 mins. The supernatant was discarded, and the final product was dispersed in 3 mL toluene.

Machine learning assisted synthesis of Yb doped $CsPbCl_3$ perovskite nanocrystals with ASC-16 ligands ($YbCl_3 \cdot 6H_2O$/TOPO): 0.123 mmol $Pb(OAc)_2 \cdot 3H_2O$, different amount of $YbCl_3 \cdot 6H_2O$ in 1mL methanol, OA, 4g TOPO and 5mL ODE were loaded in a 25 mL quartz flask. The amount of precursors and injection temperature were determined by ML model and BO. This mixture was degassed at 120 °C for 1 h until stop bubbling. Then, the flask was filled with argon and heated to a certain temperature quickly. Different amount of cesium oleate was injected swiftly and the flask was transferred to the ice bath to stop the reaction immediately. After the solution was cooled down to room temperature, the crude solution was centrifuged at 12000 rpm for 10 mins and collected the precipitate. The precipitate was dispersed in 3 mL toluene and centrifuged again at 4000 rpm for 1 min. The supernatant was centrifuged at 12000 rpm for 10 mins, and the precipitate was dispersed in 3 mL toluene. The solution was centrifuged at 4000 rpm for 1min to remove the large particles and the supernatant was used as the final colloidal solution. Ethyl acetate was employed as the antisolvent to wash the NCs' surface.

Synthesis of Yb doped $CsPbCl_3$ perovskite nanocrystals with ASC-16 ligands (oleate precursors): 0.2 mmol $Pb(OA)_2$ (400 uL), different amounts of $Yb(OA)_3$ (0.02, 0.04, 0.08, 0.16, 0.3 mmol), 5 mL ODE, ASC-16 (30mg) and 0.2 mmol cesium oleate (1.3 mL) were loaded in a 25 mL quartz flask. This mixture was degassed at room temperature for 5 mins and then heated to 110 °C under vacuum for 1 h. Then, the flask was filled with argon and increased temperature to 260 °C quickly. 0.2 mL TMS-Cl in 0.5 mL ODE was injected swiftly and the flask was transferred to the ice bath to stop the reaction. After the solution was cooled down to room temperature. The crude solution was centrifuged at 12000 rpm for 10 mins and collected the supernatant. 12 mL ethyl acetate was added into the supernatant and the mixture was centrifuged again at 12000 rpm for 10 mins. The supernatant was discarded and the final product was dispersed in 10 mL toluene.

In-situ anion exchange reaction: Diluted benzoyl bromide solution was prepared by adding 10uL benzoyl bromide in 3mL ODE in the glove box. Different amount of benzoyl bromide solution (0-20uL) was added into diluted colloidal Yb doped $CsPbCl_3$ NCs solution (OD<0.1) under the ambient conditions. Absorption and PL spectra were collected after each addition until the reaction reached completion.

PLQY measurement: The absolute photoluminescence quantum yield (PLQY) was obtained using diluted Yb doped perovskite nanocrystals dispersed in toluene (OD<0.1 at excitation wavelength) placed in a 10 mm path length quartz cuvette and fixed in a 10 cm integrating sphere (Gooch & Housego). A 375 nm continuous-wave laser was used as the excitation light to excite the samples and a neutral-density fiber was used to adjust the excitation power. The instrument responsivity including integrating sphere, optical fiber, grating, and detector was got by using a calibration lamp (OCEAN Optics, HL-3-CAL-INT). The PLQY is defined as emitted photon

number divided by the absorbed photon number. The absorbed photon number is the absorbed area between the corrected spectra of the blank toluene sample and the diluted nanocrystal sample. The emitted photon number is the integrated area of the corrected emission peak. Standard dyes were used to calibrated our PLQY setup, which aligned well with the reported values: Rhodamine 6G-measured (86.8%), literature (89.0%)[47]; IR140-measured (18.5%), literature (20.0%)[48].

Computational Details: All DFT calculations were performed using Vienna Ab initio Simulation Package (VASP, version 6.4).[49-50] The core-valence interaction is described using the projector augmented wave method[51-52], with 9 valence electrons for Cs ($5s^2 5p^6 6s^1$), 14 valence electrons for Pb ($5d^{10} 6s^2 6p^2$), 7 valence electrons for Cl ($3s^2 3p^5$), 6 electrons for S ($3s^2 3p^4$), 6 electrons for O ($2s^2 2p^4$), 5 valence electrons for N ($2s^2 2p^3$) and 4 electrons for C ($2s^2 2p^2$). The electronic wavefunctions were expanded in a planewave basis with an energy cut-off of 520 eV, and the exchange correlation was approximated by the PBE functional.[53] The Brillouin zone of the bulk cubic phase $CsPbCl_3$ was sampled with a 6 × 6 × 6 Γ-centered Monkhorst-Pack **k**-point grid.[54] The atoms were relaxed until the Hellman-Feynman forces converged below 10^{-2} eV $Å^{-1}$, and the volume is relaxed until all components of the stress tensor are below 10^{-2} GPa.

To model the interaction between the ligands and the perovskite nanocrystal surfaces, we created 3 × 3 × 4 supercells of $CsPbCl_3$ with the top and bottom surfaces being the facets terminated by CsCl. The CsCl surface termination was found to be thermodynamically more stable than the other surfaces. To prevent spurious interactions between perovskite slabs, a vacuum of 15 Å is added in the *z*-direction, with a commensurate 2 × 2 × 1 **k**-point grid for the Brillouin zone sampling. For the isolated ligands, the vacuum was added in all three spatial directions, and only the Γ point was sampled in the Brillouin zone. Three different configurations of the CsCl Schottky defect pair were created on the perovskite surfaces, with the most stable configuration used for subsequent passivation by the ligands.

The binding affinity (E_{bind}) of the ligands to the perovskite surface was computed as

$$E_{bind} = E_{tot} - E_{slab} - E_{ligand}$$

where E_{tot} is the total energy of the passivated perovskite supercell, E_{slab} is the energy of the unpassivated perovskite slab with the Schottky defect pair, and E_{ligand} is the energy of the isolated ligand. For the ligand pair of OA+OAm, the OA ligand was in the deprotonated state and the OAm ligand was in the protonated state to preserve the charge neutrality of the supercell.

Crystal structures are visualized using BLENDER[55]and BEAUTIFUL ATOMS[56].

Characterization: The PL emission from the host material was recorded by a silicon (charge-coupled device) CCD detector and the Yb emission was recorded by a liquid-nitrogen-cooled InGaAs detector. UV–vis spectra were recorded in the range of 300–600 nm by using a UV spectrometer (Shimadzu UV-3600). For photostability test, in-situ PL measurement was carried out when the colloidal solution was irradiated with UV laser at room temperature and the PL intensity as the function of irradiation time was recorded. For the thermal stability test, the colloidal solution was dropped cast on

the glass substrate and then put on the hotplate with 80 °C in the glove box. After being annealed with different time, the sample was transferred outside and cooled down to room temperature when did the steady-state PL measurement. TEM images were collected on a JEM 2010 HR machine and the accelerating voltage is 200 kV. XRD patterns were collected by drop casting highly concentrated perovskite nanocrystal solution on the glass substrate through a Bruker D8 advance diffractometer. The scan angle was set from 10 – 60° and the step size was 0.1°. The lifetime of Yb emission was obtained by irradiating the colloidal nanocrystals solution with 375 nm CW laser using 30 Hz square-wave pulses, and the NIR luminescence was detected using a silicon photodiode and recorded with a digital oscilloscope. TA spectroscopy was conducted with a HELIOS femtosecond transient absorption spectrometer (Ultrafast Systems, LLC). The pump pulse (300 nm) was generated by a Coherent Ultrafast optical parametric amplifier and the probe pulse was generated by focusing 800 nm laser on a CaF_2 crystal. The signal was recorded by a CMOS sensor within the spectrometer. Colloidal perovskite nanocrystal solutions were filled into 2 mm path-length quartz cuvettes and stirred continuously during TA measurement to avoid photo-charging. The real Yb doping concentration was determined by ICP-OES test. The purified perovskite nanocrystals were digested by diluted nitric acid overnight with sonication. The measurements were carried out with a PerkinElmer Avio 200 ICP emission spectrometer. NMR measurements were recorded on a Bruker Avance II HD Spectrometer operating at a 1H frequency of 700 MHz and equipped with a 5mm z-gradient PATXI probe.

Supporting Information

Supporting Information is available from the Wiley Online Library or from the author.

Acknowledgements

This research is supported by the National Research Foundation (NRF), Prime Minister's Office, Singapore under the Competitive Research Program (NRF-CRP25-2020-0004) and the Singapore Ministry of Education under its AcRF Tier 2 grant (MOE-T2EP50221-0035, MOE-T2EP50123-0001). Y.L. acknowledges funding support from A*STAR under its Young Achiever Award and Career Development Fund (C233312001). This work is also supported by the A*STAR Computational Resource Center (ACRC) and the National Supercomputing Centre (NSCC) through the use of their high-performance computing facilities. S.A.B. is grateful to the CEA's PTC-MP program and GENCI project AD010914188 for support.

Conflict of Interest

The authors declare no conflict of interest.

Keywords

Quantum cutting, perovskite nanocrystals, Yb doping, zwitterionic ligands, ligands engineering.

Reference

[1] D. E. Lacklison, G. B. Scott, J. L. Page, *Solid State Commun.* **1974**, 14, 861.
[2] Q. Y. Zhang, X. Y. Huang, *Prog. Mater Sci.* **2010**, 55, 353.
[3] B. M. V. D. Ende, L. Aarts, A. Meijerink, *Adv. Mater.* **2009**, 21, 3073.
[4] Oskam, KD, Wegh, RT, Donker, van, Loef, EVD, Meijerink, *J Alloys Compounds* **2000**, 300, 421.
[5] T. J. Milstein, D. M. Kroupa, D. R. Gamelin, *Nano Lett.* **2018**, 18, 3792.
[6] T. Milstein, K. Kluherz, D. Kroupa, C. S. Erickson, J. J. De Yoreo, D. R. Gamelin, *Nano Lett.* **2019**, 19, 1931.
[7] C. S. Erickson, M. J. Crane, T. J. Milstein, D. R. Gamelin, *The Journal of Physical Chemistry C* **2019**, 123, 12474.
[8] J. Y. D. Roh, T. J. Milstein, D. R. Gamelin, *ACS nano* **2023**, 17, 17190.
[9] J. Y. D. Roh, D. E. Sommer, T. J. Milstein, S. T. Dunham, D. R. Gamelin, *Chemistry of Materials* **2023**, 35, 8057.
[10] S. E. Creutz, R. Fainblat, Y. Kim, M. C. De Siena, D. R. Gamelin, *J. Am. Chem. Soc.* **2017**, 139, 11814.
[11] R. Martín-Rodríguez, R. Geitenbeek, A. Meijerink, *Journal of the American Chemical Society* **2013**, 135, 13668.
[12] N. V. Tepliakov, A. V. Sokolova, D. A. Tatarinov, X. Zhang, W. Zheng, A. P. Litvin, A. L. Rogach, *Nano Lett.* **2024**, 24, 3347.
[13] D. Zhou, D. Liu, G. Pan, X. Chen, D. Li, W. Xu, X. Bai, H. Song, *Adv. Mater.* **2017**, 29, 1704149.
[14] D. Zhou, R. Sun, W. Xu, N. Ding, D. Li, X. Chen, G. Pan, X. Bai, H. Song, *Nano Lett.* **2019**, 19, 6904.
[15] X. Shen, Z. Wang, C. Tang, X. Zhang, B. R. Lee, X. Li, D. Li, Y. Zhang, J. Hu, D. Zhao, *Nano Lett.* **2023**, 23, 82.
[16] Y.-J. Yu, C. Zou, W.-S. Shen, X. Zheng, Q.-S. Tian, Y.-J. Yu, C.-H. Chen, B. Zhao, Z.-K. Wang, D. Di, O. M. Bakr, L.-S. Liao, *Angew. Chem. Int. Ed.* **2023**, 62, e202302005.
[17] Y. Jing, K. Cao, B. Zhou, S. Geng, Y. Wen, B. Shan, R. Chen, *Chemistry of Materials* **2020**, 32, 10653.
[18] Q. Zhong, M. Cao, Y. Xu, P. Li, Y. Zhang, H. Hu, D. Yang, Y. Xu, L. Wang, Y. Li, X. Zhang, Q. Zhang, *Nano Letters* **2019**, 19, 4151.
[19] G. Almeida, L. Goldoni, Q. Akkerman, Z. Dang, A. H. Khan, S. Marras, I. Moreels, L. Manna, *ACS nano* **2018**, 12, 1704.
[20] G. Almeida, I. Infante, L. Manna, *Science* **2019**, 364, 833.
[21] J. De Roo, M. Ibanez, P. Geiregat, G. Nedelcu, W. Walravens, J. Maes, J. C. Martins, I. Van Driessche, M. V. Koyalenko, Z. Hens, *Acs Nano* **2016**, 10, 2071.
[22] J. Li, L. Xu, T. Wang, J. Song, J. Chen, J. Xue, Y. Dong, B. Cai, Q. Shan, B. Han, H. Zeng, *Adv. Mater.* **2017**, 29, 1603885.
[23] J. Song, T. Fang, J. Li, L. Xu, F. Zhang, B. Han, Q. Shan, H. Zeng, *Adv. Mater.* **2018**, 30, 1805409.
[24] D. Yang, X. Li, W. Zhou, S. Zhang, C. Meng, Y. Wu, Y. Wang, H. Zeng, *Adv. Mater.* **2019**, 31, 1900767.

[25] F. Krieg, S. T. Ochsenbein, S. Yakunin, S. ten Brinck, P. Aellen, A. Süess, B. Clerc, D. Guggisberg, O. Nazarenko, Y. Shynkarenko, S. Kumar, C.-J. Shih, I. Infante, M. V. Kovalenko, *ACS Energy Letters* **2018**, 3, 641.
[26] F. Montanarella, K. M. McCall, K. Sakhatskyi, S. Yakunin, P. Trtik, C. Bernasconi, I. Cherniukh, D. Mannes, M. I. Bodnarchuk, M. Strobl, B. Walfort, M. V. Kovalenko, *ACS Energy Letters* **2021**, 6, 4365.
[27] F. Krieg, Q. K. Ong, M. Burian, G. Rainò, D. Naumenko, H. Amenitsch, A. Süess, M. J. Grotevent, F. Krumeich, M. I. Bodnarchuk, I. Shorubalko, F. Stellacci, M. V. Kovalenko, *J. Am. Chem. Soc.* **2019**, 141, 19839.
[28] V. Morad, A. Stelmakh, M. Svyrydenko, L. G. Feld, S. C. Boehme, M. Aebli, J. Affolter, C. J. Kaul, N. J. Schrenker, S. Bals, Y. Sahin, D. N. Dirin, I. Cherniukh, G. Raino, A. Baumketner, M. V. Kovalenko, *Nature* **2024**, 626, 542.
[29] T. A. Cohen, Y. Huang, N. A. Bricker, C. S. Juhl, T. J. Milstein, J. D. MacKenzie, C. K. Luscombe, D. R. Gamelin, *Chem. Mater.* **2021**, 33, 3779.
[30] T. J. Milstein, D. M. Kroupa, D. R. Gamelin, *Nano Lett* **2018**, 18, 3792.
[31] X. Shen, Z. Wang, C. Tang, X. Zhang, B. R. Lee, X. Li, D. Li, Y. Zhang, J. Hu, D. Zhao, F. Zhang, W. W. Yu, B. Dong, X. Bai, *Nano Lett* **2023**, 23, 82.
[32] C. S. Erickson, M. J. Crane, T. J. Milstein, D. R. Gamelin, *The Journal of Physical Chemistry C* **2019**, 123, 12474.
[33] G. Almeida, O. J. Ashton, L. Goldoni, D. Maggioni, U. Petralanda, N. Mishra, Q. A. Akkerman, I. Infante, H. J. Snaith, L. Manna, *Journal of the American Chemical Society* **2018**, 140, 14878.
[34] Y. Hou, J. Shi, W. Chu, Z. Sun, *Eur. J. Inorg. Chem.* **2013**, 2013, 3063.
[35] F. Krieg, S. T. Ochsenbein, S. Yakunin, S. Ten Brinck, P. Aellen, A. Süess, B. Clerc, D. Guggisberg, O. Nazarenko, Y. Shynkarenko, *ACS energy letters* **2018**, 3, 641.
[36] A. K. Low, F. Mekki-Berrada, A. Ostudin, J. Xie, E. Vissol-Gaudin, Y.-F. Lim, A. Gupta, Q. Li, Y. S. Ong, S. A. Khan, **2023**.
[37] B. P. MacLeod, F. G. Parlane, C. C. Rupnow, K. E. Dettelbach, M. S. Elliott, T. D. Morrissey, T. H. Haley, O. Proskurin, M. B. Rooney, N. Taherimakhsousi, *Nature communications* **2022**, 13, 995.
[38] L. Cao, D. Russo, K. Felton, D. Salley, A. Sharma, G. Keenan, W. Mauer, H. Gao, L. Cronin, A. A. Lapkin, *Cell Reports Physical Science* **2021**, 2, 100295.
[39] C. E. Rasmussen, in *Summer school on machine learning*, Springer, 2003.
[40] D. E. Sommer, D. R. Gamelin, S. T. Dunham, *Physical Review Materials* **2022**, 6, 025404.
[41] J. Aneesh, A. Swarnkar, V. Kumar Ravi, R. Sharma, A. Nag, K. Adarsh, *The Journal of Physical Chemistry C* **2017**, 121, 4734.
[42] T. J. Milstein, K. T. Kluherz, D. M. Kroupa, C. S. Erickson, J. J. De Yoreo, D. R. Gamelin, *Nano letters* **2019**, 19, 1931.
[43] D. Zhou, D. Liu, G. Pan, X. Chen, D. Li, W. Xu, X. Bai, H. Song, *Adv Mater* **2017**, 29, 1704149.
[44] N. Ding, W. Xu, D. Zhou, Y. Ji, Y. Wang, R. Sun, X. Bai, J. Zhou, H. Song, *Nano Energy* **2020**, 78, 105278.
[45] X. Luo, T. Ding, X. Liu, Y. Liu, K. Wu, *Nano Lett* **2019**, 19, 338.
[46] T. A. Cohen, Y. Huang, N. A. Bricker, C. S. Juhl, T. J. Milstein, J. D. MacKenzie, C. K. Luscombe, D. R. Gamelin, *Chemistry of Materials* **2021**, 33, 3779.
[47] C. Würth, M. Grabolle, J. Pauli, M. Spieles, U. Resch-Genger, *Analytical chemistry* **2011**, 83, 3431.

[48] S. Hatami, C. Würth, M. Kaiser, S. Leubner, S. Gabriel, L. Bahrig, V. Lesnyak, J. Pauli, N. Gaponik, A. Eychmüller, *Nanoscale* **2015**, 7, 133.
[49] G. Kresse, J. Furthmüller, *Physical review B* **1996**, 54, 11169.
[50] G. Kresse, J. Furthmüller, *Computational materials science* **1996**, 6, 15.
[51] P. E. Blöchl, *Physical review B* **1994**, 50, 17953.
[52] G. Kresse, D. Joubert, *Physical review b* **1999**, 59, 1758.
[53] J. P. Perdew, K. Burke, M. Ernzerhof, *Physical review letters* **1996**, 77, 3865.
[54] H. J. Monkhorst, J. D. Pack, *Physical review B* **1976**, 13, 5188.
[55] O. Blender, *Retrieved. represents the sequence of Constructs1 to* **2018**, 4.
[56] X. Wang, T. Tian, A. Ulrich. Beautiful Atoms: A python library for the manipulation and visualization of atomistic structure using blender, **2022.**